Modelling and Impact of Hydraulic Short Circuit Operation in Pumped Hydro Energy Storage

Inga Beyers[1] Lukas Krebeck[1] Astrid Bensmann[1] Richard Hanke-Rauschenbach[1]

[1]Leibniz University Hannover, Institute of Electric Power Systems, Appelstraße 9A, 30167 Hannover, Germany

Abstract

This paper investigates the hydraulic short circuit (HSC) operation of pumped hydro energy storage systems, specifically how it can be modelled and its impact on energy capacity, efficiency and operating range. Hydraulic short circuit operation enables power modulation during charging for fixed-speed pumped hydro systems, thereby allowing them to operate more flexibly. In this work, a pumped hydro storage system with 140.5 MW nominal charging power and 10 h nominal charging time is analysed. The storage is simulated via a dynamic, system-level model composed of detailed physical component models to accurately depict the HSC operating behaviour. HSC enables part-load operation from 39 MW to 107 MW but with significantly lower overall system efficiencies. The HSC operating limits are governed by the turbine's minimum flow and maximum power. The custom-built OpenModelica library employed for this analysis can be downloaded from `https://github.com/ibeyers/pumped-storage-lib`.

Keywords: energy storage, pumped hydro, hydraulic short circuit, flexibility, off-design operation

1 Introduction

This paper focuses on the hydraulic short circuit operation mode of pumped hydro energy storage systems. The role and operation of pumped hydro energy storage in the European electricity system have changed following the liberalisation of energy markets and the increasing integration of fluctuating renewable energy sources. Moving away from traditional arbitrage operation, pumped hydro systems now often participate in multiple markets and generate additional revenue from ancillary services, such as frequency regulation (Pérez-Díaz et al. 2015). As a consequence, the operational flexibility of pumped hydro storage systems has become a key focus area in the field of pumped hydro research and practice (Giese and Magnoli 2019). This is an issue because the operational flexibility of traditional fixed-speed pumped hydro is severely limited on the charging side. Since the power consumption of a fixed-speed pump is governed by the system head, deliberate power modulation is not possible during charging (Valavi and Nysveen 2018)[1]. Pumped hydro operators increasingly retrofit existing systems to enable more operational flexibility, while flexibility is already a central design consideration for new systems (Vagoni et al. 2024).

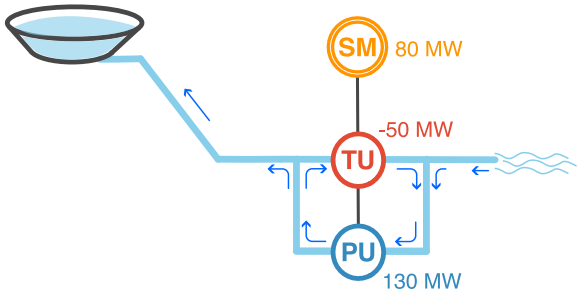

Figure 1. Illustration of hydraulic short circuit operation in a ternary machine set (pump, turbine and synchronous machine). During charging, a part of the flow is recirculated to the turbine, which delivers power and therefore reduces the system's net power consumption.

One approach to counteract this inflexibility and enable deliberate power modulation during charging is the so-called "hydraulic short circuit" (HSC) operation. Here, a portion of the pumping flow is redirected to a turbine, whose power delivery can be adjusted via the guide vane opening. This allows the system's net power consumption to be regulated by adjusting the turbine power delivery. This principle is illustrated in Figure 1. This mode requires at least two hydraulic machines, either in a single ternary machine set or two pump-turbines, with one operating as a pump and the other as a turbine. The advantage of HSC is that it can be retrofitted with relatively low capital expenditure, while the disadvantage is the low system efficiency (Vagoni et al. 2024). We recently investigated the operational flexibility and performance of different pumped hydro configurations, including HSC operation (Beyers, Krebeck, et al. 2025). In this work, we build on that previous work but focus on three aspects of hydraulic short circuit not yet addressed in the literature.

The first aspect is the implementation of the library, which was developed to simulate pumped hydro systems and HSC operation in the OpenModelica environment (Fritzson et al. 2020). Pumped storage research is

[1]Strictly speaking, it is not impossible but rather not advisable. Theoretically, pump throttling can be used to achieve a degree of freedom in pump operation (Alizadeh Bidgoli, Yang, and Ahmadian 2020). However, the resulting damage to the pump is unacceptable and pump throttling, therefore, does not feature in the continuous operation of pumped hydro storage systems

often conducted using proprietary software, and the results are then shared without a deeper insight into the underlying methodology and implementation, see, e.g. Ruppert et al. (2017) and Geiger and Riedelbauch (2023). Open source modelling can therefore contribute to open research and accelerate R&D efforts in this field. A well-executed open hydropower library for Modelica (OpenHPL) developed by Vytvytskyi (2019) exists; however, it currently cannot model the bidirectional operation of pumped hydro. Therefore, a custom library was developed[2]. The second aspect is an elaboration of the flow regimes that ensue during HSC operation. So far, the HSC mechanism in the entire hydraulic network has not been demonstrated in detail in the literature. By understanding the HSC mechanism, the impact of HSC operation on energy capacity, efficiency and operating range can be demonstrated very clearly. The third aspect is extending HSC with a thermal analysis. Practical experience at the Frades II pumped hydro plant has shown that hydraulic short circuit operation can lead to inadmissibly high water temperatures since the losses of the hydraulic machines heat up the circulating water (Pinto et al. 2024). This could significantly impact continuous operation and make HSC less suitable for retrofits of certain pumped hydro system types. To the authors' best knowledge, this aspect has never been formally investigated and therefore, warrants a first exploration.

Our paper will, therefore, deliver the following three contributions:

1. Focus on implementation aspects of modelling HSC.
2. A more detailed elaboration of flow regimes during HSC operation.
3. An investigation of non-isothermal HSC.

This paper is structured as follows: Section 2 details the system under consideration. Section 3 presents an overview of the methodology, including the implementation in a custom-built OpenModelica library. Section 4 presents the results and Section 5 concludes this work.

2 System under consideration

The system analysed in this work is a synthetic pumped hydro system. This is done to avoid a case-specific bias and instead develop general-purpose insights. The hydraulic scenario is taken from previous work (Beyers, Krebeck, et al. 2025). Key characteristics are:

- Upper reservoir with a geodetic head $\overline{h}_{\mathrm{geo}}$ of the reservoir water level ranging from 480 m (empty) to 520 m (full).
- Circular upper reservoir with tapered walls, with an opening angle of 30°.
- Upper reservoir sized so that 100 MW can be delivered for 10 h.
- Lower reservoir with an infinite capacity, such as a river or lake, which acts as a boundary with a constant head.
- Total waterway distance of 2.4 km.

The 500 m average geodetic head is explicitly chosen to keep this a generic scenario where all technical configurations are viable.

Within this hydraulic scenario, we consider a single ternary machine set with a dedicated pump and a Francis turbine. The machine set shaft is connected to a salient-pole synchronous machine. A block transformer steps up the synchronous machine voltage to the grid voltage (or steps down, depending on the direction of power flow). The hydraulic and electrical machines are sized to deliver 100 MW nominal discharging power and consume 140.5 MW nominal charging power at the grid connection point with a power factor $\cos(\varphi)$ of 0.9. In contrast to the previous paper, the machines here are sized for a symmetric charging and discharging duration of 10 h, resulting in higher charging power. Key parameters are summarised in Table 1.

Table 1. Selected parameters of hydraulic and electrical machines.

Component	*Parameter*	*Value*
Transformer	Nom. apparent power $S_{\mathrm{tr}}^{\mathrm{nom}}$	156 MVA
	Nom. high voltage $U_{\mathrm{tr,hv}}^{\mathrm{nom}}$	220 kV
Synchronous Machine	Nom. apparent power $S_{\mathrm{sm}}^{\mathrm{nom}}$	156 MVA
	Nom. stator voltage $U_{\mathrm{sm,st}}^{\mathrm{nom}}$	10.5 kV
	Nom. rotor speed $n_{\mathrm{sm,ro}}^{\mathrm{nom}}$	500 rpm
Turbine	Number of stages N_{s}	1
	Specific speed of stage $n_{\mathrm{q,tu}}^{\mathrm{nom}}$	24.0
Pump	Number of stages N_{s}	2
	Specific speed of stage $n_{\mathrm{q,pu}}^{\mathrm{nom}}$	41.0

3 Methodology

This section is divided into three parts: Section 3.1 describes the general modelling approach, Section 3.2 presents an overview of the components, and Section 3.3 discusses select aspects of the pumped storage library.

3.1 Modelling approach

In this work, we employ a system-level model formulation to account for all machines and their interactions up to the grid connection point. The model combines dynamic components and quasi-stationary components. The components are connected to each other to form a system model. Because the focus is on continuous operation, the system's dynamics are governed by the reservoir. The

[2]It should be noted that the library is currently under development. Its purpose is to answer the specific questions pursued by the authors and therefore does not cover all aspects of pumped hydro storage.

DOI 10.3384/ecp218353

filling and emptying of the reservoir result in a head variation, which forces the rest of the components into off-design operation. Faster dynamics (e.g., the inertia of rotating masses in machines) can be neglected compared to the slow dynamics of the reservoir. The other component models are therefore considered quasi-stationary; they undergo a sequence of stationary operating points set by the dynamic reservoir head variation. The system is simulated with a so-called "hot start" at nominal speed, i.e. the start-up sequence from standstill is not modelled. The passive sign convention is used in this work. Quantities flowing into a component (or the system) are positive, whereas quantities flowing out are negative. At the grid connection point, charging power is positive and discharging power is negative.

3.2 Component models

Our previous publication (Beyers, Krebeck, et al. 2025) describes the component models in detail. This section briefly reiterates key aspects.

Upper reservoir, conduits and point losses. The hydraulic waterway elements and the hydraulic machines are all characterised by head h and volumetric flow q, as is common in the field of fluid systems. The head is the total mechanical energy of a flow, expressed in a height in meters:

$$h = \frac{p(t)}{\rho g} + \frac{v(t)^2}{2g} + h_{\text{geo}} \tag{1}$$

It is composed of the pressure head $p(t)/\rho g$, the velocity head $v(t)^2/2g$ and geodetic head h_{geo}. Water is considered an incompressible medium with a constant density of $\rho = 1000\,\text{kg/m}^3$.

The reservoir is governed by a dynamic mass balance, expressed here through the reservoir volume V_{ur}:

$$\frac{\mathrm{d}V_{\text{ur}}}{\mathrm{d}t} = q(t) \tag{2}$$

The reservoir is characterised by a State-of-Charge (SOC) that relates the volume contained in the reservoir to the nominal water volume:

$$\text{SOC}(t) = \frac{V_{\text{ur}}(t)}{V_{\text{ur}}^{\text{nom}}} \tag{3}$$

The water volume in the upper reservoir and the water level $x(t)$ are linked through the geometric shape of the reservoir.

$$V_{\text{ur}}(t) = \frac{x(t)\cdot\pi}{3}\cdot\left(R(t)^2 + R(t)\cdot r + r^2\right) \tag{4}$$

with the radius at the bottom r and the top of the water volume $R(t) = r + x(t)\cdot\tan(30^\circ)$.

The components through which the water is transported are either conduits (distributed "pipe" elements such as the headrace, the penstock and the tailrace) or point losses, which include all other elements, (e.g., intake, rake, bends) that incur *local* losses. They are modelled as lumped, static components with conservation of mass and energy[3]. Conservation of energy is expressed through the extended Bernoulli equation (Pritchard and Leylegian 2011), which includes losses in the form of a friction head h_{fric}:

$$h_{\text{in}}(t) = h_{\text{out}}(t) + h_{\text{fric}}(t) \tag{5}$$

In this formulation, the change in internal thermal energy of the water through the friction losses is neglected. The friction head for the conduits with the length l, diameter d and friction factor $\lambda(t)$ is:

$$h_{\text{fric}}(t) = \lambda(t)\cdot\frac{l}{d}\cdot\frac{v(t)\cdot|v(t)|}{2g} \tag{6}$$

For the point losses the term $\lambda(t)\cdot\frac{l}{d}$ is replaced by an empirical friction factor ζ specific to each component.

Hydraulic machines. The hydraulic machines are modelled with mechanistic models, which combine Euler equations that reflect ideal machine behaviour with empirical/semi-empirical loss models. The pump model is based on Tuzson (2000), and the turbine model is from Nielsen (2015) and Reines and Svingen (2020).

To demonstrate the models, the parameterised pump and turbine performance maps are shown in Figure 2 a) (pump) and Figure 2 b) (turbine). Figure 2 a) contains the pump curves, plotting head over volumetric flow rate, combined with isolines for speed (dash-dotted) and relative efficiency (solid). The pump always operates at best guide vane opening, eliminating this variable from the pump map. The turbine map in b) is visualised differently since the adjustable guide vane opening offers an additional degree of freedom in operation. The map plots the volumetric flow rate over the turbine speed, with isolines of the same guide vane opening (dashed) and relative efficiency (solid). The turbine performance map is shown for the nominal head.

Electrical machines. Both the synchronous machine and the transformer are modelled with complex phasor equivalent circuit models (ECM), with constant parameters. This is a standard modelling procedure to describe stationary and quasi-stationary behaviour. It is described in reference works, such as Müller and Ponick (2009) and Oeding and Oswald (2016). The synchronous machine has an internal-voltage-based equivalent circuit model. It is complemented by separate loss functions, e.g., for iron losses (Engevik, Valavi, and Nysveen 2016), windage losses and additional losses (Pyrhönen, Jokinen, and Hrabovcová 2013).

[3]For steady, incompressible flow along a streamline, conservation of momentum leads to the same expression as conservation of energy (Pritchard and Leylegian 2011)

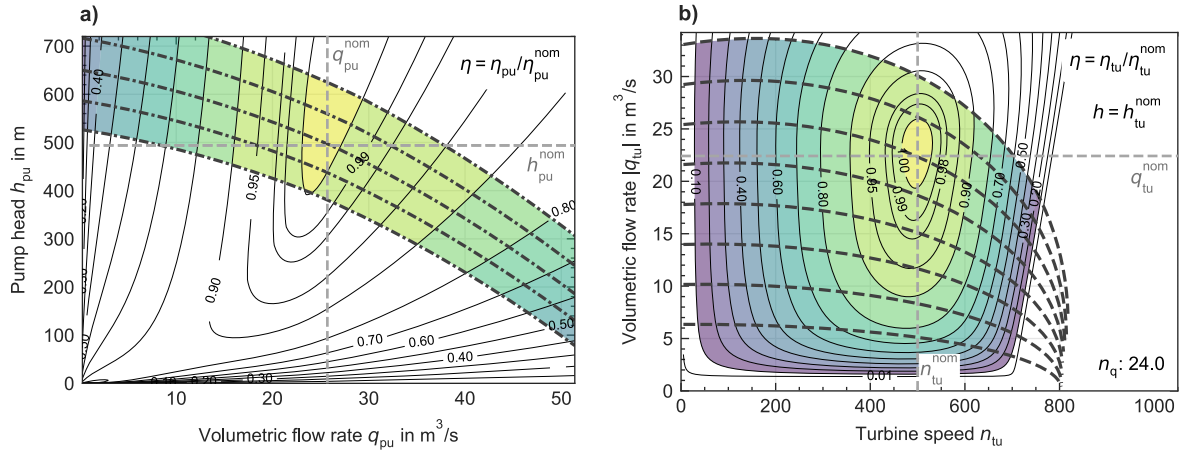

Figure 2. Parameterised pump model in a) and turbine model in b), shwon as performance maps. In the pump map, the dash-dotted curves are isolines of the same speed. The solid lines are isolines for the relative efficiency $\eta_{pu}/\eta_{pu}^{nom}$. In the turbine map, the dashed curves are isolines of the same guide vane opening. The solid lines are isolines for the relative efficiency $\eta_{tu}/\eta_{tu}^{nom}$.

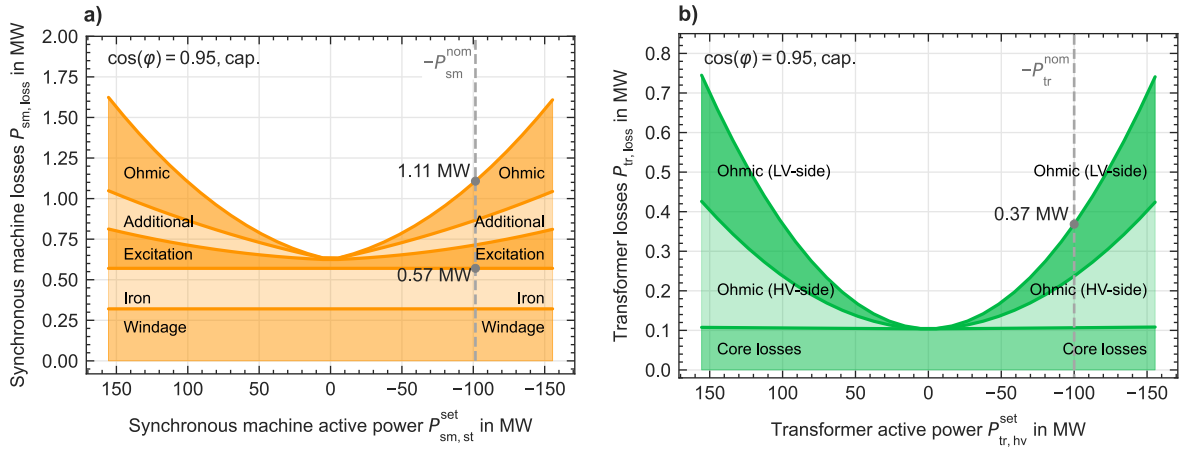

Figure 3. Loss breakdown of the parameterised synchronous machine model in a) and transformer model in b). Synchronous machine losses are plotted as a function of the active power on the stator side, $P_{sm,st}$, while the transformer losses are plotted as a function of the active power on the high-voltage side, $P_{tr,hv}$.

To provide insight into the model, Figure 3 a) shows the losses of the parameterised synchronous machine. The losses are plotted over the stator-side active power $P_{sm,st}$ at a capacitive power factor of $\cos(\varphi) = 0.95$ and nominal speed. The left side of the figure shows the motor mode (positive values, power drawn by the SM) and on the right side is the generator mode (negative values, power delivered by the SM). The losses are non-linear. At nominal discharging power, approximately 51 % of losses are constant losses (windage, iron) and 49 % are load-dependent.

The transformer is modelled with a T-shaped equivalent circuit model. The T-ECM includes a shunt element, which represents the core losses and causes a significant efficiency drop in low part-load. To illustrate the model's behaviour, the losses of the parameterised transformer are shown in Figure 3 b). The losses are plotted over the high-voltage-side active power $P_{tr,hv}$ at a capacitive power factor of $\cos(\varphi) = 0.95$. The losses are dominated by the Ohmic losses at nominal discharging power.

3.3 Implementation in a custom OpenModelica library

For this analysis, a custom-built OpenModelica library is employed, making use of the features of the Modelica language, i.e. multi-physics, equation-based and object-oriented modelling. General-purpose libraries lack required components for this analysis (e.g. a salient-pole synchronous machine) and are not necessarily parameterised for the scale of pumped hydro components. Therefore, the component models have been developed from the ground up to meet the specific modelling needs and model depth required. However, the custom models use the Modelica standard library for, e.g., units, icons, control elements, and connectors. The parameterisation of the component models is performed in separate Python scripts, where the resulting parameter sets are then copied to OpenModelica. The models used for this analysis are found in a subpackage called "ModelicaConference2025".

DOI 10.3384/ecp218353

Key aspects of the library are discussed in the following paragraphs.

The hydraulic elements, such as conduits, point losses and reservoirs, are modelled in an *acausal* manner. This has the advantage that a single model representation can be used for all modes of operation since the flow direction is not prescribed. This is important, as flow direction can vary between regular charging, regular discharging and hydraulic short circuit operation.

The library uses Modelica's object-oriented nature. There are four separate model layers: component models, subsystem models, full system models, and the control layer. The smallest unit is a component, where a "flat" model formulation is used. The hydraulic components are instantiated to build a hydraulic subsystem, referred to as the "waterway." The lower reservoir is a sink, and only the head is specified as a boundary condition. The waterway is then extended by the conversion machines (pump, turbine, synchronous machine, and transformer) to form a full system. Separating the waterway from the conversion machines has the advantage that different machine types and sizes can be tested in the same hydraulic system. Finally, the control layer is added by extending the full system, so that experimentation with different control strategies is possible. Where possible, ideal controllers in the form of implicit equations are implemented. Where explicit control loops are necessary, such as setting the turbine power to achieve a specified power at the grid connection point during HSC, they are implemented as PID (proportional-integral-derivative) control.

The full system model is shown in Figure 4. The shaft power outputs and inputs from the hydraulic machines are connected to the synchronous machine with causal input/output connectors. The electrical machines are only connected via causal input/output connectors, each with a set of connectors for power consumption and delivery. They are connected via sum-to-zero coupling of active and reactive power. The full system model includes auxiliary losses, which are modelled as an active power loss between synchronous machine and transformer. During discharging, the active power is set at the grid connection point and the power requirements are propagated back through the transformer and synchronous machine to the turbine component. During charging, the active power required by the pump is propagated in the other direction towards the grid connection point. The reactive power is determined from the active power at the grid connection point via a constant power factor in operation of 0.95 and communicated back to the synchronous machine component. In hydraulic short circuit operation, the turbine power is controlled via a PID controller to maintain the constant charging power setpoint at the grid connection.

4 Results and Discussion

The results are divided into four subsections. Section 4.1 analyses the impact of HSC operation at a single point in time, focusing on the flow conditions, the power split between machines, and the resulting efficiency. In Section 4.2, an entire HSC charging process is simulated over time. In Section 4.3, multiple HSC and regular charging/discharging processes are aggregated to quantify the system's energy capacity-power relationship, efficiency-power relationship, and operating range. Finally, Section 4.4 contains a brief consideration of the thermal behaviour.

4.1 Hydraulic short circuit operation at different power levels

To elaborate on the effects of HSC operation, the flow conditions and further variables are shown for two snapshots in time for 50 MW and 60 MW part-load charging, respectively, at a SOC of 0.5. Figure 5 is for a charging power of 50 MW at the grid connection point. At a SOC of 0.5, 50 % of the nominal water mass is stored in the reservoir and the total reservoir head is 502.77 m (comprising 480 m elevation at the reservoir bottom and a water level of 22.77 m). Recall that the head in the upper reservoir varies between 480 m (empty) and 520 m (full), yielding a relative water level of $22.77\,\mathrm{m}/40\,\mathrm{m} = 56.9\%$. Due to the tapered geometry, the relative water level and SOC differ.

The head values are shown in red at every connection point between two components. This is the total head from the extended Bernoulli equation, composed of pressure head, velocity head and geodetic head. These three contribute differently depending on the location in the waterway, but the proportions are not detailed here. Furthermore, the constant water level of the lower reservoir is set to $h = 0\,\mathrm{m}$, thus the total head is given relative to this reference level. The head difference between different points of the waterway displayed in Figure 5 is thus solely due to the friction losses in the conduits and fittings.

The pump has a power consumption of 134.55 MW at nominal speed and a pump head of $h_{\mathrm{pu}} = 504.91\,\mathrm{m}$. The resultant flow in this operating point is $24.8\,\mathrm{m}^3/\mathrm{s}$. The flow values are printed in blue above or beside the relevant conduits. The turbine needs to deliver -86.16 MW to the shaft to achieve 50 MW active power consumption by the transformer at the grid connection point. For this, $19.5\,\mathrm{m}^3/\mathrm{s}$ of the flow is redirected to the turbine. Only the remaining $5.3\,\mathrm{m}^3/\mathrm{s}$ flows up to the reservoir. Because of the low net flow in large parts of the waterway, the head losses are also comparatively low. For reference, in regular charging/discharging operation the head loss due to friction is $> 10\,\mathrm{m}$. In this HSC operating point, the pump must overcome only $504.91\,\mathrm{m} - 502.77\,\mathrm{m} = 2.15\,\mathrm{m}$ of total friction head loss for the entire waterway.

The net shaft power supplied by the synchronous machine rotor is 48.39 MW. The losses of the synchronous machine, the auxiliary losses, and the transformer losses are added to yield a total active power consumption of $P_{\mathrm{gc}} = 50\,\mathrm{MW}$ at the grid connection point. The total system efficiency can be calculated by dividing the hydraulic power flowing into the reservoir P_{ur} by the active power

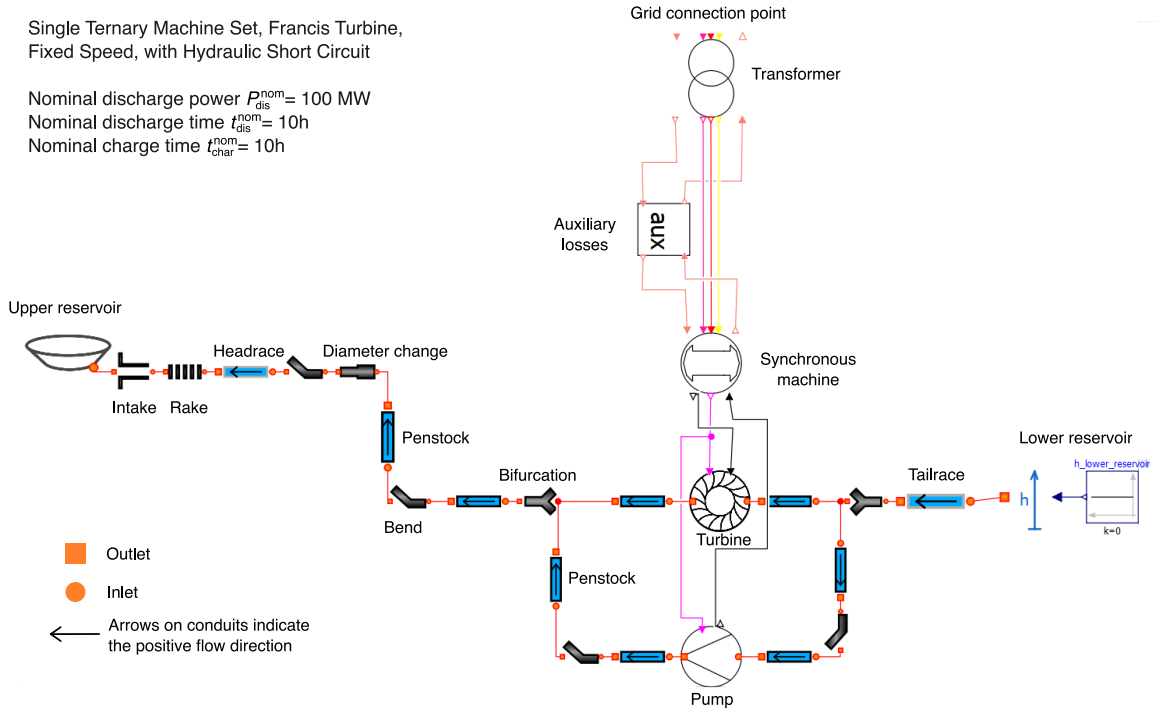

Figure 4. Full system model as implemented in OpenModelica. Note that because this is an abstract representation of the pumped hydro system, the dimensions of the waterway are not to scale.

supplied at the grid connection point P_{gc}:

$$\eta_{sys}(t) = \frac{P_{ur}(t)}{P_{gc}(t)} \tag{7}$$

with $P_{ur}(t) = h_{ur}(t) \cdot q(t) \cdot g \cdot \rho$. This operating point achieves an efficiency of 52.28 %, which is relatively low compared to efficiencies achieved in normal charging or discharging operations. It is important to note that the hydraulic short circuit efficiency cannot be estimated by multiplying all the component efficiencies because the power flow is not unidirectional. In hydraulic short circuit, there are two opposing power flows, each with its associated losses, which is the reason for the low total system efficiency. Figure 6 shows the same variables for 60 MW part-load and a SOC of 0.5, so the upper reservoir head ($h_{ur} = 502.77$ m) is identical to that in Figure 5. Conceptually, part-load charging with HSC is the same for 50 MW and 60 MW, however, three key aspects are highlighted below to better understand HSC operation. The first aspect is the complementary relationship between turbine power and charging power: a *low* HSC charging power (more part-load) requires higher turbine output (more negative power), while a high HSC charging power (less part-load) requires lower absolute turbine power. The second aspect is that the system efficiency is strongly influenced by the proportion of flow recirculated through the turbine. At 60 MW HSC charging power, less flow is recirculated through the turbine than at 50 MW ($17.3\,m^3/s$ vs. $19.5\,m^3/s$). Thus, more net flow reaches the upper reservoir, and the system efficiency is ultimately higher. The higher the flow through the turbine, the lower the system efficiency. Thirdly, the pump operating point is slightly different at 60 MW and SOC = 0.5 than at 50 MW and SOC = 0.5 because of the head friction losses. The headrace and the long diagonal penstock are the main drivers of the head friction losses. At 60 MW, the flow through these conduits is slightly higher, incurring higher losses, requiring the pump to supply a higher head (505.49 m vs 504.91 m at 50 MW). This shifts the pump operating point upwards and to the left on the pump curve (refer to Figure 2 a), which means the pump flow is slightly lower at $24.7\,m^3/s$ vs. $24.8\,m^3/s$ at 50 MW.

4.2 Hydraulic short circuit operation over time

Figure 7 demonstrates a complete 50 MW, constant-power HSC charging process over time to showcase the system dynamics. The simulation takes 4.6 s of computation time using a time step of 10 s. The upper reservoir starts at SOC = 0 and is terminated at SOC = 1 with a charging time of 44.5 hours. Figure 7 a) shows the pump head (solid line) and flow (dashed line) on the y-axis over the charging time on the x-axis. The main dynamic is the water level variation in the upper reservoir. Consequently, as the charging progresses, the pump sees an increasing head from 482.5 m to 521.8 m as the reservoir is filled and the water level rises. As the head increases, the pump flow decreases. On the pump curve (refer back to Figure 2 a), this corresponds to a leftward shift along the curve. The pump power consumption is largely governed by the pump flow.

DOI 10.3384/ecp218353

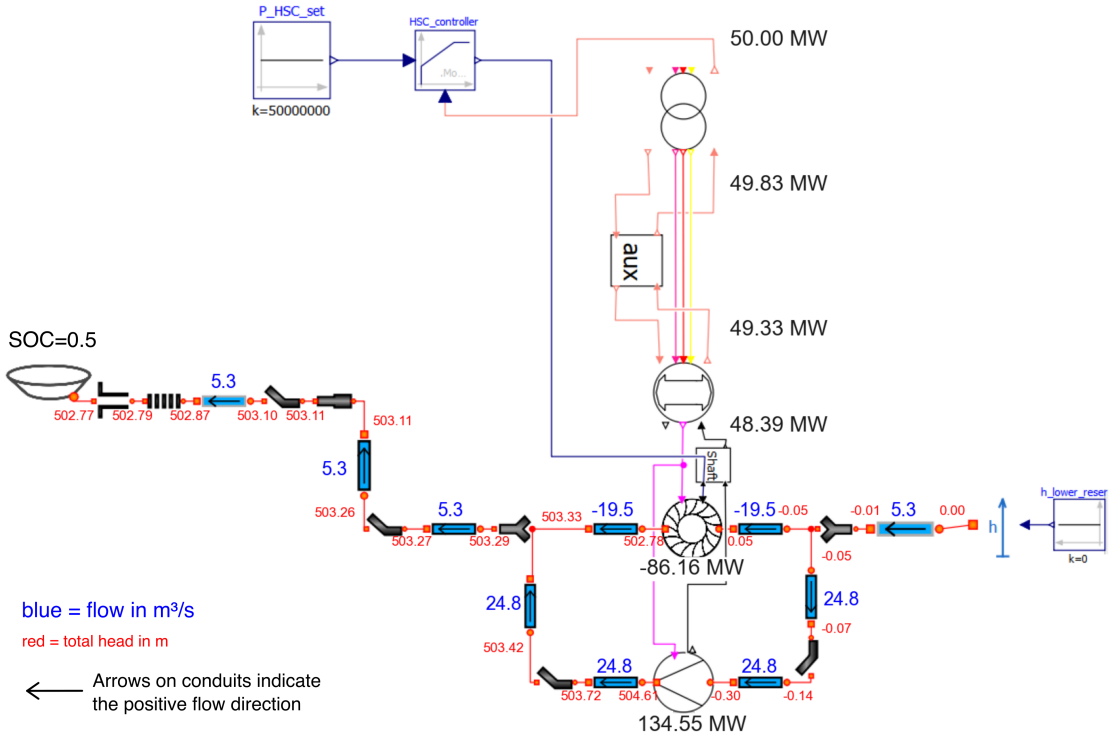

Figure 5. Snapshot in time of key variables of the pumped storage system during hydraulic short circuit operation. State-of-Charge is 0.5 and the charging power at the grid connection point is 50 MW. The flow values are printed in blue above or beside the relevant conduits. The head values are printed in red at every connection point between two components. The power values are printed in black next to the machines.

Therefore, as the flow decreases, the pump power at the shaft $P_{\mathrm{pu,sh}}$, shown in blue in Figure 7 b), decreases as well from 142.6 MW (start) to 128.1 MW (end). To achieve a constant power consumption of 50 MW at the grid connection point, the turbine power is controlled accordingly, by adjusting the guide vane opening. As shown in the red curve in Figure 7, the absolute turbine power $|P|_{\mathrm{tu,sh}}$ decreases with the pump power, enabling a constant power supply at the rotor of the synchronous machine ($P_{\mathrm{sm,ro}}$ in yellow). The total system efficiency is shown in Figure 7 c). The system efficiency starts at 50.7 %, achieves a maximum value of 52.4 % at 27.7 hours and then drops to 51.7% at the end.

4.3 Energy capacity, efficiency and operating range of the pumped hydro system.

Depending on the power supplied to or discharged from the system, the pumped storage system has a different energy capacity and system efficiency. These are referred to as the energy-power ($E-P$) and efficiency-power ($\eta-P$) relationships, which are presented and discussed in this section. To visualise these relationships, we employ the Ragone plot framework (Beyers, Bensmann, and Hanke-Rauschenbach 2023), which is briefly reiterated here. A constant-power charging process is simulated, starting from an empty system at SOC=0 and continuing until the process is terminated. Two quantities are computed from the charging process: the electrical energy capacity, calculated as $E = \int_0^{t=t_{\mathrm{end}}} P_{\mathrm{gc}} \mathrm{d}t$, and the average system efficiency, calculated as $\overline{\eta}_{\mathrm{sys}} = \int_0^{t=t_{\mathrm{end}}} \eta_{\mathrm{sys}} \mathrm{d}t / t_{\mathrm{end}}$. This process is repeated for a different P_{c} = constant charging power. All the capacity and average efficiency values are then combined and plotted in a single curve. The procedure for discharging is the same, except that the constant-power discharging starts at a SOC of 1 and continues until termination.

Figure 8 plots the resulting $\eta-P$ and $E-P$ curves versus the full range of possible charging/discharging powers on the x-axis. Regarding the visual presentation, the charging side is shown on the left, and the discharging is on the right. The x-axis ranges from high charging powers (left) to high discharging powers (right), with 0 MW at the center. Figure 8 a) shows the average efficiency $\overline{\eta}_{\mathrm{sys}}$. The first insight is that not all power levels are possible. The operating range is discontinuous, and there are three separate elements in the $\eta-P$ curve, each belonging to a mode of operation. The modes are annotated as follows: "1P" is charging with one pump, "1P1T" is the hydraulic short circuit charging with one pump and one turbine simultaneously, and "1T" is discharging with one turbine. 1T is possible between -36.1 MW and -102.9 MW. The system efficiency is generally high but drops in part-load and over-load. A charging part-load lower than 36.1 MW is not possible, because the turbine component has an built-in flow limit of $q_{\mathrm{tu}}^{\mathrm{min}} = 0.4 \cdot q_{\mathrm{tu}}^{\mathrm{nom}}$ to avoid cavitation phenomena in part-load (Pereira Jr. et al. 2019). Over-load is

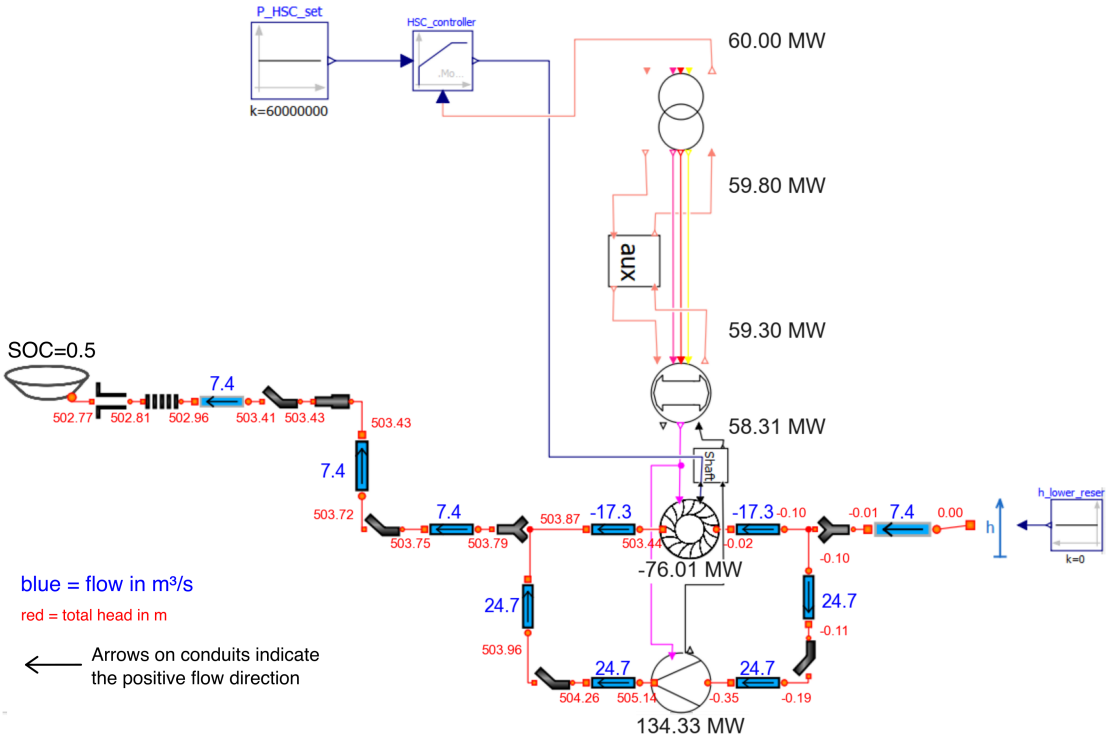

Figure 6. Snapshot in time of key variables of the pumped storage system during hydraulic short circuit operation. State-of-Charge is 0.5 and the charging power at the grid connection point is 60 MW. The flow values are printed in blue above or beside the relevant conduits. The head values are printed in red at every connection point between two components. The power values are printed in black next to the machines.

limited by the maximum turbine power of -105 MW.

Regular charging only with the pump (1P) does not comply with the constant-power framework since power variation is always present in fixed-speed configurations. To include regular charging anyway, its average power is shown as a single dot to distinguish it conceptually from the constant-power 1P1T and 1T operation. Hydraulic short circuit charging (1P1T) is possible between 39.8 MW and 107.1 MW. As discussed in Section 4.1, the efficiencies are generally lower than in regular operation and decrease further in part-load as more flow is diverted to the turbine. The turbine governs the HSC operating range. Because of the opposing relationship between turbine power and HSC charging power, the *minimum* HSC charging power of 39.8 MW is set by the *maximum* turbine power and the *maximum* HSC charging power of 107.1 MW is limited by the *minimum* turbine flow.

Figure 8 b) shows the energy capacity added to the system (charging) or removed from the system (discharging). E and P are linked by the charging/discharging duration. In Figure 8 b), dashed isochrone lines with varying slopes are plotted to mark points in the $E-P$ plane with identical charging/discharging durations. As a further reference, the energy stored in the full upper reservoir at SOC $= 1$ is plotted as a horizontal solid line. In discharging operation (1T), less energy capacity can be taken from the system than stored in the upper reservoir. In charging operation (1P), more energy capacity must be added to the system than ends up in the reservoir. In HSC operation (1P1T), the energy capacity curve has a pronounced turning point at 90.6 MW, which is not reflected in the efficiency curve. To understand this, recall that during a constant-power HSC charging process, the turbine power is continually lowered to match the lowering pump power (refer to Figure 7). At power values higher than 90.6 MW, the charging process is terminated prematurely because the minimum flow limit of the turbine is reached. The higher the HSC charging power, the earlier this limit is reached. Therefore, the capacity that can be added to the system drops until $P_{gc} = 107.1$ MW, which can only be supplied for 10 minutes[4].

In summary, HSC allows operational flexibility in part-load but at a significantly reduced efficiency. At higher HSC charging powers (closer to full load), the charging processes are cut short, significantly reducing charging energy capacity. At deeper part-load, the average system efficiency drops significantly.

4.4 Non-isothermal hydraulic short circuit operation

The original model formulation does not consider thermal effects since they are negligible during regular operation.

[4] Although E theoretically approaches zero, this is not considered relevant for continuous operation.

DOI 10.3384/ecp218353

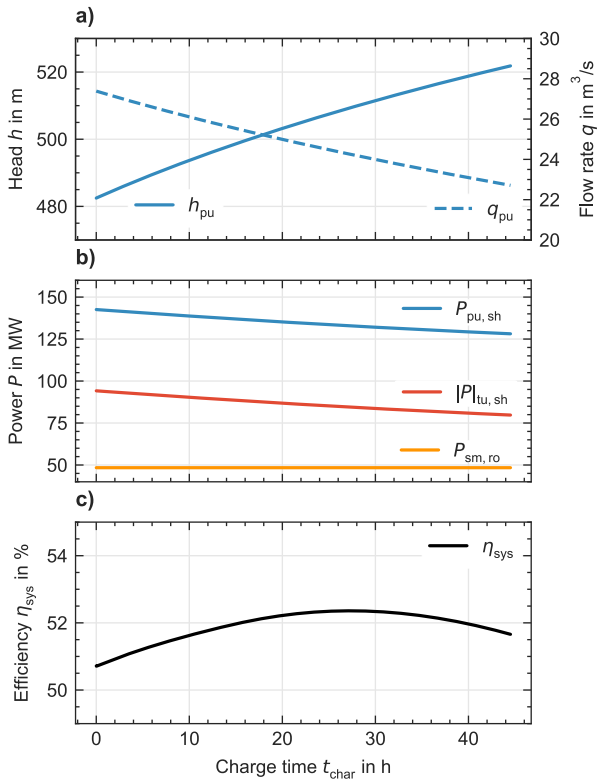

Figure 7. HSC operation at a charging power of $P_{gc} = 50\,\text{MW}$ simulated over time. Subfigure a) shows pump head and volume flow rate, b) shows the power values of turbine, pump and synchronous machine, while c) shows the system efficiency.

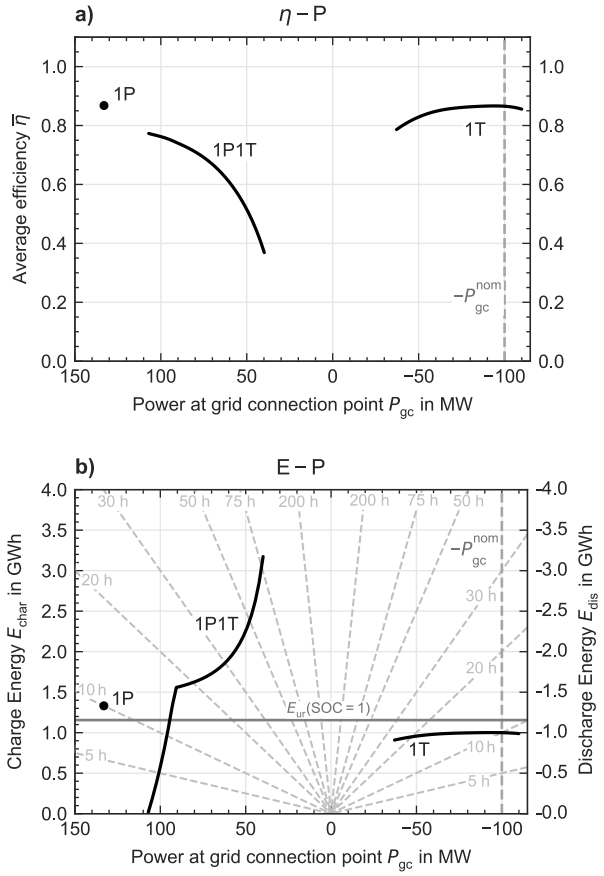

Figure 8. Efficiency-power ($\eta - P$) curves in a) and energy-power ($E - P$) curves in b) of the pumped hydro system at hand.

However, in a hydraulic short circuit, the water circulating between the machines can heat up to unacceptably high temperatures. An energy balance considering the internal thermal energy of the water is incorporated into the model to explore the thermal effects. For simplicity, we consider the entire pipe network of the hydraulic short circuit loop around the ternary machine set as a single control volume with a uniform temperature. In this control volume, the water mass is assumed constant since the incoming flow from the lower reservoir equals the outgoing flow to the upper reservoir and the variation in water density is negligible. The assumption of a uniform temperature in the HSC loop is an approximation, but the flow speeds are so large within the HSC loop that they override local effects on the timescales under analysis. The energy balance, assuming a constant water density, is:

$$m_{\text{HSC}} \cdot c_p \cdot \frac{dT_{\text{HSC}}}{\text{d}t} = \dot{m}_{\text{in}} \cdot c_p \cdot T_{\text{in}} + \dot{m}_{\text{out}} \cdot c_p \cdot T_{\text{HSC}} + P_{\text{loss,pu}} + P_{\text{loss,tu}} + P_{\text{fric}}. \quad (8)$$

The final temperature for a complete HSC charging process at $P_{gc} = 60\,\text{MW}$ is 20.72°C. For 50 MW, this becomes 21.05°C; for 39 MW, the final temperature in the HSC loop is 21.98°C. Therefore thermal effects are not an issue in the operating range determined by the machine sizing. The magnitude of the flow out of the HSC loop towards the upper reservoir is large enough to transport heat generated by losses away. A test in which the same system is equipped with a larger turbine reveals that the temperature within the HSC loop only becomes critical as flow toward the upper reservoir approaches zero. In that case, the relatively small water mass within in the HSC loop start notably accumulating the heat from machine losses since the heat is not transported away and into the upper reservoir. Critical temperatures exceeding 80°C are reached.

5 Conclusions and Outlook

This work developed a detailed physical model of a fixed-speed pumped hydro storage system with 100 MW nominal discharging power and a nominal charging and discharging duration of 10 hours. A hydraulic short circuit between the pump and the turbine was implemented to enable flexibility during charging operation. The effects of hydraulic short circuit operation were demonstrated both with instantaneous values and continuous operation over longer time periods. Instantaneous analysis of two different power levels (50 MW and 60 MW) highlights the complex component interactions during HSC operation. We recommend adopting the level of detail in this work for modelling HSC operating behaviour, specifically (i) an

accurate waterway network representation, (ii) hydraulic machine models with off-design performance relations, and (iii) consideration of the reservoir head variation. The system has a low efficiency in HSC operation. Therefore, strong economic incentives are needed for this mode of operation.

Several constant-power charging and discharging process simulations over time were combined to form $E-P$ and $\eta-P$ curves. This analysis shows that the operating range of the pumped storage system is not continuous. HSC enables part load charging between 39.8 MW and 107.1 MW. The HSC operating range is constrained by the turbine's maximum power and minimum flow limits. This should be considered when designing new pumped hydro systems. The available energy capacity drops significantly at HSC charging powers > 93 MW, a trend not apparent from the $\eta-P$ curve alone. This highlights the need to complement investigations of system efficiency with the energy capacity perspective.

The thermal analysis shows that HSC operation has only a small, negligible effect on the circulating water temperature in this specific pumped storage system. A brief investigation indicates that the temperature only becomes critical around flow regimes approaching zero flow towards the upper reservoir. Thermal considerations become relevant only when the pump and turbine powers are more evenly matched, and low flows towards the upper reservoirs are feasible operating points.

Overall, model-based investigations, such as the one conducted here, can reveal the operational flexibility potential of existing pumped hydro installations and systems in planning, thereby enabling these systems to contribute even more to modern decarbonised energy systems.

References

Alizadeh Bidgoli, Mohsen, Weijia Yang, and Ali Ahmadian (2020). "DFIM versus synchronous machine for variable speed pumped storage hydropower plants: A comparative evaluation of technical performance". In: *Renewable Energy* 159, pp. 72–86. DOI: 10.1016/j.renene.2020.05.163.

Beyers, Inga, Astrid Bensmann, and Richard Hanke-Rauschenbach (2023). "Ragone plots revisited: A review of methodology and application across energy storage technologies". In: *Journal of Energy Storage* 73, p. 109097. DOI: 10.1016/j.est.2023.109097.

Beyers, Inga, Lukas Krebeck, et al. (2025). *Comparing Operational Flexibility and Performance of Pumped Hydro Energy Storage Systems: A Quantitative Analysis of Technology Options*. Preprint available at SSRN. DOI: 10.2139/ssrn.5355183.

Engevik, Erlend L., Mostafa Valavi, and Arne Nysveen (2016). "Efficiency and loss calculations in design of converter-fed synchronous hydrogenerators". In: *2016 XXII International Conference on Electrical Machines (ICEM)*, pp. 1636–1642. DOI: 10.1109/ICELMACH.2016.7732743.

Fritzson, Peter et al. (2020). "The OpenModelica Integrated Environment for Modeling, Simulation, and Model-Based Development". en. In: *Modeling, Identification and Control: A Norwegian Research Bulletin* 41.4, pp. 241–295. ISSN: 0332-7353, 1890-1328. DOI: 10.4173/mic.2020.4.1.

Geiger, Christoph and Stefan Riedelbauch (2023). "Power Plant Transients including Hydraulic Short Circuit Operation Mode". In: *Energies* 16.11, p. 4492. DOI: 10.3390/en16114492.

Giese, Martin and Marcelo Magnoli (2019). *Recent Developments of Hydropower Machines for Pumped Storage Projects*. URL: https://cdn2.hubspot.net/hubfs/5069195/Voith-NA-Files/Voith-Developments-Hydro-PumpedStorage-2019.pdf.

Müller, Germar and Bernd Ponick (2009). *Grundlagen elektrischer Maschinen*. de. 9th ed. 1. Weinheim: John Wiley & Sons, Ltd. ISBN: 978-3-527-40524-4. URL: https://onlinelibrary.wiley.com/doi/abs/10.1002/352760782X.ch.

Nielsen, Torbjørn K (2015-09). "Simulation model for Francis and Reversible Pump Turbines". In: *International Journal of Fluid Machinery and Systems* 8.3, p. 14. DOI: 10.5293/IJFMS.202015.8.3.169.

Oeding, Dietrich and Bernd R. Oswald (2016). *Elektrische Kraftwerke und Netze*. de. 8th ed. Berlin, Heidelberg: Springer Vieweg. DOI: 10.1007/978-3-662-52703-0.

Pereira Jr., João Gomes et al. (2019-10). "Procedure for predicting part load resonance in Francis turbine hydropower units based on swirl number and local cavitation coefficient similitude". In: *Mechanical Systems and Signal Processing* 132, pp. 84–101. DOI: 10.1016/j.ymssp.2019.06.011.

Pérez-Díaz, Juan I. et al. (2015). "Trends and challenges in the operation of pumped-storage hydropower plants". In: *Renewable and Sustainable Energy Reviews* 44, pp. 767–784. DOI: 10.1016/j.rser.2015.01.029.

Pinto, Pedro Diogo et al. (2024). *Combining Technologies: Variable Speed And Hydraulic Short Circuit*. Lausanne.

Pritchard, Philip J. and John C. Leylegian (2011). *Fox and McDonald's Introduction to Fluid Mechanics*. 8th. John Wiley & Sons, Inc. ISBN: 978-0-470-54755-7.

Pyrhönen, Juha, Tapani Jokinen, and Valéria Hrabovcová (2013). "Losses and Heat Transfer". In: *Design of Rotating Electrical Machines*. Section: 9. John Wiley & Sons, Ltd, pp. 523–569. ISBN: 978-1-118-70159-1. DOI: 10.1002/9781118701591.ch9.

Reines, A F and B Svingen (2020). "Analysis and improvement of a mathematical turbine model". In: *Journal of Physics: Conference Series* 1608.1, p. 012001. DOI: 10.1088/1742-6596/1608/1/012001.

Ruppert, Leopold et al. (2017). "An analysis of different pumped storage schemes from a technological and economic perspective". In: *Energy* 141, pp. 368–379. DOI: 10.1016/j.energy.2017.09.057.

Tuzson, John (2000). *Centrifugal Pump Design*. Wiley. ISBN: 978-0-471-36100-8.

Vagoni, E. et al. (2024). *Technical White Paper, XFLEX HYDRO Project*. Tech. rep. Deliverable D10.3. EPFL. URL: https://www.xflexhydro.com/knowledge/technical-white-paper#downloads.

Valavi, Mostafa and Arne Nysveen (2018). "Variable-Speed Operation of Hydropower Plants: A Look at the Past, Present, and Future". In: *IEEE Industry Applications Magazine* 24.5, pp. 18–27. DOI: 10.1109/MIAS.2017.2740467.

Vytvytskyi, Liubomyr (2019). "Dynamics and model analysis of hydropower systems". PhD thesis. Porsgrunn: University of South-Eastern Norway. URL: http://hdl.handle.net/11250/2608105.